JOURNAL OF THE KOREAN ASTRONOMICAL SOCIETY
34: S209 ~ S213, 2001

Magnetohydrodynamics Code Basics

DONGSU RYU
Department of Astronomy & Space Science, Chungnam National University, Daejon 305-764, Korea
(Received Sep. 1, 2001; Accepted Nov. 15, 2001)

ABSTRACT

This paper describes the numerical solution to the hyperbolic system of magnetohydrodynamic (MHD) equations. First, by pointing out the approximations involved, the deal MHD equations are presented. Next, the MHD waves as well as the associated shocks and discontinuities, are presented. Then, based on the hyperbolicity of the ideal MHD equations, the application of upwind schemes, which have been developed for hydrodynamics, is discussed to solve the equations numerically. As an definite example, one and multi-dimensional codes based on the Total Variation Diminishing scheme are presented. The treatment in the multi-dimensional code, which maintains $\nabla \cdot \boldsymbol{B} = 0$, is described. Through tests, the robustness of the upwind schemes for MHDs is demonstrated.

Key Words : methods: numerical — MHD

I. Introduction

Computational astrophysics has been drived not only by dramatic advances in computer hardwares, but also by comparable developments in improved algorithms. Recent progresses in methods to solve the equations of compressible magnetohydrodynamics (MHDs) are particularly important. It is not only because that system is the most applicable to describe a vast array of central astrophysical problems, but also because MHDs presents a special challenge due to the complexity by three non-isotropically propagating wave families with wide ranging relative characteristic speeds.

Conservative, Riemann-solver-based schemes, which are inherently upwind, have proven to be very effective for solving MHD equations as well as hydrodynamic equations. The upwind schemes share an ability to sharply and cleanly define fluid discontinuities, especially shocks, and exhibit a robustness that makes them broadly applicable. These schemes conservatively update the zone-averaged or grid-centered fluid and magnetic field states based on estimated advective fluxes of mass, momentum, energy and magnetic field at grid interfaces using solutions to the Riemann problem at each interface. MHD examples include Brio & Wu (1988), Zachary & Colella (1992), Zachary, *et al.* (1994), Dai & Woodward (1994a,1994b), Powell (1994), Powell *et al.* (1995), Ryu & Jones (1995), Ryu, *et al.* (1995), Roe & Balsara (1996), Balsara (1998), Tóth (1997), Kim *et al.* (1999), and Jiang & Wu (1999). Brio & Wu applied the Roe's approach to the MHD equations. Zachary and collaborators used the BCT scheme to estimate fluxes, while Dai & Woodward applied the PPM scheme to MHDs. Powell and collaborators developed a Roe-type Riemann solver with an eight-wave structure for MHDs. Ryu and collaborators extended the Harten's TVD scheme to MHDs. Balsara and Tóth used also a TVD scheme to build an MHD code. Kim and collaborators built a code for the MHD equations with the isothermal equation of state based on a TVD scheme. Jiang & Wu applied an ENO scheme to MHDs.

The feature of upwind schemes that grid-centered quantities are used to estimate fluxes at grid interfaces makes enforcing $\nabla \cdot \boldsymbol{B} = 0$ non-trivial. As the result, the explicit divergence-cleaning scheme, which restricts the choice of boundary conditions, has been used at first (see *e.g.*, Ryu, *et al.* 1995). However, recently Dai & Woodward (1998), Ryu *et al.* (1998), Balsara & Spicer (1999), and Londrillo & Del Zanna (2000) succeeded in incorporating the staggered mesh technique in upwind schemes, which assures $\nabla \cdot \boldsymbol{B} = 0$.

II. Ideal Magnetohydrodynamics

(a) Equations

MHDs describes the behavior of the combined system of a conducting fluid and magnetic fields in the limit that the displacement current and the separation between ions and electrons are neglected. So, the MHD equations represent coupling of the equations of fluid dynamics with the Maxwell's equations of electrodynamics. When the effects of electrical resistivity, viscosity, and thermal conductivity are dropped, the following ideal MHD equations are obtained,

$$\frac{\partial \rho}{\partial t} + \nabla \cdot (\rho \boldsymbol{v}) = 0, \tag{1}$$

$$\frac{\partial \boldsymbol{v}}{\partial t} + \boldsymbol{v} \cdot \nabla \boldsymbol{v} + \frac{1}{\rho} \nabla p - \frac{1}{\rho} (\nabla \times \boldsymbol{B}) \times \boldsymbol{B} = 0, \tag{2}$$

$$\frac{\partial p}{\partial t} + \boldsymbol{v} \cdot \nabla p + \gamma p \nabla \cdot \boldsymbol{v} = 0, \tag{3}$$

$$\frac{\partial \boldsymbol{B}}{\partial t} - \nabla \times (\boldsymbol{v} \times \boldsymbol{B}) = 0. \tag{4}$$

Here, we have chosen units so that factor of 4π does not appear in the equations. An additional explicit constraint $\nabla \cdot \boldsymbol{B} = 0$ is imposed to account for the absence of magnetic monopoles.

(b) Waves

While disturbances in a neural gas are propagated by sound waves, a magnetized and electrically conducting medium can support more than one kinds waves. In order to study them, let us take the unperturbed state of the medium to be static and homogeneous:

$$\rho_o = \text{const.}, \quad \boldsymbol{v}_o = 0, \quad p_o = \text{const.}, \quad \boldsymbol{B}_o = \text{const}, \tag{5}$$

and consider small perturbations of this system:

$$\rho = \rho_o + \delta\rho, \quad \boldsymbol{v} = \delta\boldsymbol{v}, \quad p = p_o + \delta p, \quad \boldsymbol{B}_o = \boldsymbol{B}_o + \delta\boldsymbol{B}. \tag{6}$$

We can look for normal mode solutions having the following form for the perturbed quantities:

$$\delta Q \propto e^{i(\omega t - kx)}. \tag{7}$$

By substituting Eq. (5)-(7) in the MHD equations and linearizing for the perturbed quantities, the dispersion relation is obtained:

$$\omega(\omega^2 - c_a^2)(\omega^2 - c_f^2)(\omega^2 - c_s^2) = 0, \tag{8}$$

where

$$c_a = \sqrt{\frac{B_x^2}{\rho}}, \tag{9}$$

$$c_f = \left[\frac{1}{2}\left\{a^2 + \frac{B^2}{\rho} + \sqrt{\left(a^2 + \frac{B^2}{\rho}\right)^2 - 4a^2\frac{B_x^2}{\rho}}\right\}\right]^{\frac{1}{2}}, \tag{10}$$

$$c_s = \left[\frac{1}{2}\left\{a^2 + \frac{B^2}{\rho} - \sqrt{\left(a^2 + \frac{B^2}{\rho}\right)^2 - 4a^2\frac{B_x^2}{\rho}}\right\}\right]^{\frac{1}{2}}, \tag{11}$$

are the speeds of Alfvén, fast, and slow waves respectively. Here, a is the speed of sound wave given by

$$a = \sqrt{\gamma\frac{p}{\rho}}. \tag{12}$$

The Alfvén wave is a transverse wave with $\delta\rho = 0$ (that is, incompressible). On the other hand, the fast and slow waves have $\delta\rho \neq 0$ (that is, compressible) as the sound wave in hydrodynamics. The wave speeds have the following order

$$c_f \geq c_a \geq c_s. \tag{13}$$

(c) Shocks and Discontinuities

Since MHD flows have three kinds of waves, we expect several shocks and discontinuities. Shocks and discontinuities are described by the following jump conditions, which are derived from the conservative form of the MHD equations (see the next section):

$$[\rho v_x] = 0, \tag{14}$$

$$\left[\rho v_x^2 + p + \frac{1}{2}B_\parallel^2 - \frac{1}{2}B_x^2\right] = 0, \tag{15}$$

$$[\rho v_x \boldsymbol{v}_\parallel - B_x\boldsymbol{B}_\parallel] = 0, \tag{16}$$

$$\left[\left(\frac{1}{2}\rho v^2 + \frac{\gamma}{\gamma-1}p + B^2\right)v_x - (\boldsymbol{B}\cdot\boldsymbol{v})\,B_x\right] = 0, \tag{17}$$

$$[B_x] = 0, \tag{18}$$

$$[v_x\boldsymbol{B}_\parallel - B_x\boldsymbol{v}_\parallel] = 0, \tag{19}$$

where shocks and discontinuities are assumed to propagate along the x-direction and the subscript $\parallel$ denotes the direction perpendicular to the propagation.

Each of the three MHD waves as well as the entropy mode (represented by ω in the dispersion relation, Eq. 8) has a nonlinear counterpart. The fast wave is associated with the fast shock which has across the shock the characteristics of

$$B_x = \text{continuous}, \quad |\boldsymbol{B}_\parallel|_{\text{postshock}} > |\boldsymbol{B}_\parallel|_{\text{preshock}}, \tag{20}$$

in addition to those of hydrodynamic shocks. The slow wave is associated with the slow shock which has

$$B_x = \text{continuous}, \quad |\boldsymbol{B}_\parallel|_{\text{postshock}} < |\boldsymbol{B}_\parallel|_{\text{preshock}}. \tag{21}$$

The counterpart of the Alfvén wave is the rotational discontinuity, where all MHD quantities are continuous expect the direction of $\boldsymbol{B}_\parallel$. The counterpart of the entropy mode is the contact discontinuity, as in hydrodynamics, where where all quantities are continuous except density.

III. A Magnetohydrodynamic Code

(a) Hyperbolic Equations

In Cartesian geometry, the ideal MHD equations are written in conservative form as

$$\frac{\partial\boldsymbol{q}}{\partial t} + \frac{\partial\boldsymbol{F}_x}{\partial x} + \frac{\partial\boldsymbol{F}_y}{\partial y} + \frac{\partial\boldsymbol{F}_z}{\partial z} = 0, \tag{22}$$

$$\boldsymbol{q} = \begin{pmatrix} \rho \\ \rho v_x \\ \rho v_y \\ \rho v_z \\ B_x \\ B_y \\ B_z \\ E \end{pmatrix}, \tag{23}$$

$$\boldsymbol{F}_x = \begin{pmatrix} \rho v_x \\ \rho v_x^2 + p^* - B_x^2 \\ \rho v_x v_y - B_x B_y \\ \rho v_x v_z - B_x B_z \\ 0 \\ B_y v_x - B_x v_y \\ B_z v_x - B_x v_z \\ (E + p^*)v_x - B_x(B_x v_x + B_y v_y + B_z v_z) \end{pmatrix}, \tag{24}$$

with $\boldsymbol{F}_y$ and $\boldsymbol{F}_z$ obtained by properly permuting indices. The total pressure and the total energy are given by

$$p^* = p + \frac{1}{2}\left(B_x^2 + B_y^2 + B_z^2\right), \tag{25}$$

$$E = \frac{1}{2}\rho\left(v_x^2 + v_y^2 + v_z^2\right) + \frac{p}{\gamma - 1} + \frac{1}{2}\left(B_x^2 + B_y^2 + B_z^2\right). \tag{26}$$

With the state vector, $\boldsymbol{q}$, and the flux functions, $\boldsymbol{F}_x(\boldsymbol{q})$, $\boldsymbol{F}_y(\boldsymbol{q})$, and $\boldsymbol{F}_z(\boldsymbol{q})$, the Jacobian matrices, $\boldsymbol{A}_x(\boldsymbol{q}) = \partial\boldsymbol{F}_x/\partial\boldsymbol{q}$, $\boldsymbol{A}_y(\boldsymbol{q}) = \partial\boldsymbol{F}_y/\partial\boldsymbol{q}$, and $\boldsymbol{A}_z(\boldsymbol{q}) = \partial\boldsymbol{F}_z/\partial\boldsymbol{q}$, are formed. The system of equations is called *hyperbolic* if all the eigenvalues of the Jacobian matrices are real and distinct and the corresponding set of right eigenvectors is complete. The MHD equations form a *non-strictly hyperbolic* system, meaning that some eigenvalues may coincide at some points (see *e.g.,* Brio & Wu 1998).

Any scheme to solve a set of hyperbolic equations can be utilized to build an MHD code Here, as an illustration, a code based on the Harten's Total Variation Diminishing (TVD) scheme (Harten 1983), which is a second-order-accurate extension of the Roe-type upwind scheme (Roe 1981), is described.

(b) A One-Dimensional Code

The procedure to build a one-dimensional MHD code based on the TVD scheme is described in detail in Ryu & Jones (1995). Here, it is briefly summarized. To start, we consider a plane-symmetric, one-dimensional flow exhibiting variation along the x-direction. The first step to build the code is to find the eigenvalues and the right and left eigenvectors of the Jacobian matrix, $\boldsymbol{A}_x(\boldsymbol{q})$. The seven eigenvalues $a_1, \cdots, a_7$ in non-increasing order are

$$a_{1,7} = v_x \pm c_f, \quad a_{2,6} = v_x \pm c_a, \quad a_{3,5} = v_x \pm c_s, \quad a_4 = v_x. \tag{27}$$

The quantities $a_1, \cdots, a_7$ represent the seven characteristic speeds with which information is propagated locally by three MHD wave families and an entropy mode. The corresponding eigenvectors are given, for example, in Ryu & Jones (1995).

In a code based on the TVD scheme, the physical quantities are referred to the grid centers while the fluxes are computed on the grid interfaces. Implementation of Roe's linearization technique would result in a particular averaged form of the physical quantities on the grid interfaces (Roe 1981). But it is not possible to derive this particular analytic form of the averaged quantities in MHD for general cases with an adiabatic index $\gamma \neq 2$. Instead, we modify Roe's scheme and use $\rho_{i+\frac{1}{2}}$, $v_{x,i+\frac{1}{2}}$, $v_{y,i+\frac{1}{2}}$, $v_{z,i+\frac{1}{2}}$, $B_{y,i+\frac{1}{2}}$, $B_{z,i+\frac{1}{2}}$, $p^*_{i+\frac{1}{2}}$ on the grid interfaces with the arithmetic averages at i and $i+1$. Then, other quantities like momentum, gas pressure, total energy, etc are calculated by combining those quantities.

The state vector $\boldsymbol{q}^n$ at the time step n is updated by calculating the modified flux $\bar{\boldsymbol{f}}_x$ at the grid interfaces as follows:

$$L_x\boldsymbol{q}_i^n = \boldsymbol{q}_i^n - \frac{\Delta t^n}{\Delta x}(\bar{\boldsymbol{f}}_{x,i+\frac{1}{2}} - \bar{\boldsymbol{f}}_{x,i-\frac{1}{2}}). \tag{28}$$

The procedure to compute it is described in details in Ryu & Jones (1995). The time step Δt^n is restricted by the usual Courant condition for the stability, $\Delta t^n = C_{\rm cour}\Delta x/{\rm Max}(|v^n_{x,i+\frac{1}{2}}| + c^n_{f,i+\frac{1}{2}})$ with $C_{\rm cour} < 1$.

(c) Multi-Dimensional Extension

The multi-dimensional extension can done through a Strang-type directional splitting (Ryu *et al.* 1995). In each time step, multi-dimensional derivatives are split into a set of one-dimensional derivatives, with variations in other directions ignored temporarily. Then, each row in the grid is treated as if it were a one-dimensional problem. Updating the flow quantities along each row is done using the one-dimensional code described in the previous subsection. The parallel (to the direction of the row) component of magnetic field is kept constant and only the perpendicular component is updated. One complete time step updating the full state vector $\boldsymbol{q}^n$ to $\boldsymbol{q}^{n+1}$ in each grid cell is composed of updating it along two or three directions, as appropriate. For instance, in three-dimensional Cartesian geometry, the state vector is updated along x, y, and z-directions, so

$$\boldsymbol{q}^{n+1} = L_zL_yL_x\boldsymbol{q}^n. \tag{29}$$

In order to maintain second-order accuracy, the order of directional passes is permuted by the Strang-type prescription: $L_zL_yL_x$, $L_xL_yL_z$, $L_xL_zL_y$, $L_yL_zL_x$, $L_yL_xL_z$, and then $L_zL_xL_y$, for example. The time step is restricted to satisfy the Courant condition along each row in three directions. It is calculated at the start of the above permuting sequence and used through one complete sequence.

(d) $\nabla \cdot \boldsymbol{B} = 0$

The staggered mesh technique can be incorporated to ensure $\nabla \cdot \boldsymbol{B} = 0$. We describe the magnetic field update step in two-dimensional plane-parallel geometry (Ryu *et al.* 1998). Extensions to three-dimension and other geometries are trivial. Here, we define the magnetic field components on grid interfaces, $b_{x,i,j}$ and $b_{y,i,j}$, while all the other fluid quantities are still defined at grid centers. For use in the step of calculating the advective fluxes by the TVD scheme, the magnetic field components at grid centers, which are intermediate variables, are interpolated as

$$B_{x,i,j} = \frac{1}{2}\left(b_{x,i,j} + b_{x,i-1,j}\right), \tag{30}$$

and

$$B_{y,i,j} = \frac{1}{2}\left(b_{y,i,j} + b_{y,i,j-1}\right). \tag{31}$$

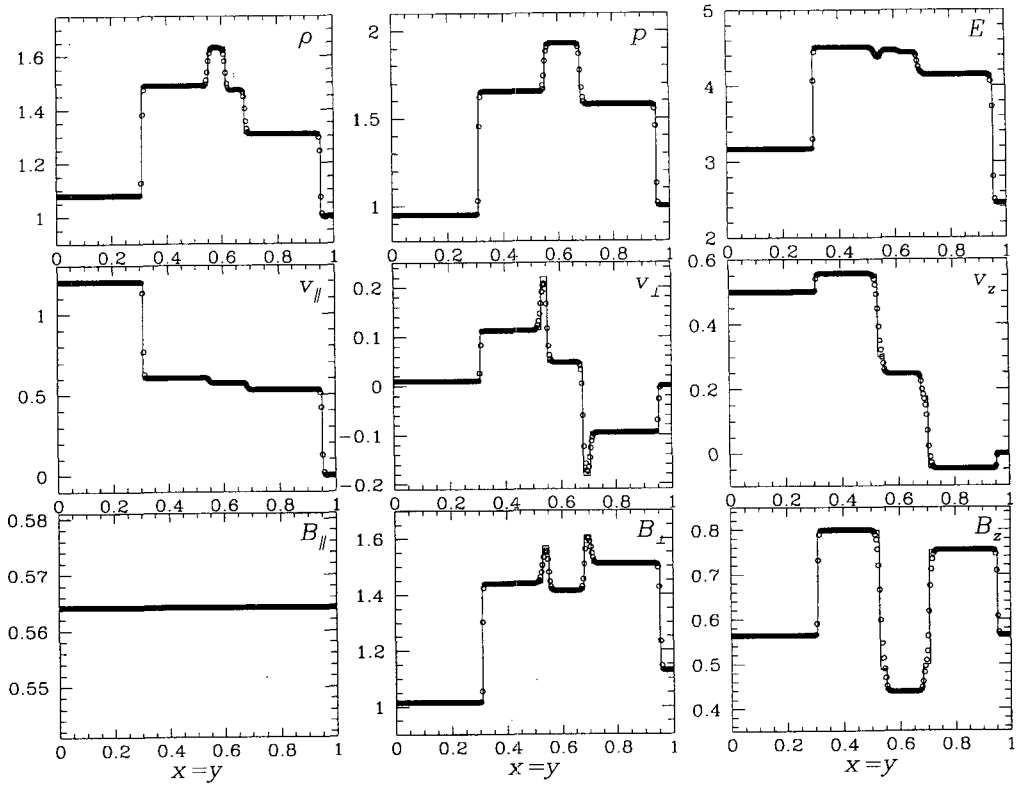

Fig. 1.— Two-dimensional MHD shock tube test.

Since the MHD code based on the TVD scheme has second-order accuracy, the above second-order interpolation should be adequate. If non-uniform grids are used, an appropriate interpolation of second-order should be used.

Using the modified fluxes at grid interfaces (§III.b), the advective fluxes, or the z-component of the electric field, on grid edges are calculated by a simple arithmetic average, which still keeps second-order accuracy: namely,

$$\bar{\Omega}_{i,j} = \frac{1}{2}\left(\bar{f}_{y,i+1,j} + \bar{f}_{y,i,j}\right) - \frac{1}{2}\left(\bar{f}_{x,i,j+1} + \bar{f}_{x,i,j}\right). \quad (32)$$

Then, the magnetic field components are updated as

$$b^{n+1}_{x,i,j} = b^{n}_{x,i,j} - \frac{\Delta t^n}{\Delta y}\left(\bar{\Omega}_{i,j} - \bar{\Omega}_{i,j-1}\right), \quad (33)$$

and

$$b^{n+1}_{y,i,j} = b^{n}_{y,i,j} + \frac{\Delta t^n}{\Delta x}\left(\bar{\Omega}_{i,j} - \bar{\Omega}_{i-1,j}\right). \quad (34)$$

Note that the $\bar{\Omega}$ terms include information from all seven characteristic modes. It is also clear that the net magnetic flux across grid interfaces is exactly kept to be zero at the step $n+1$

$$\oint_S \vec{b}^{n+1} \cdot d\vec{S} = \quad (35)$$
$$(b^{n+1}_{x,i,j} - b^{n+1}_{x,i-1,j})\Delta y + (b^{n+1}_{y,i,j} - b^{n+1}_{y,i,j-1})\Delta x = 0,$$

if it is zero at the step n.

IV. Numerical Tests

In all the tests shown, we used the adiabatic index $\gamma = 5/3$ and a Courant constant $C_{cour} = 0.8$.

(a) Shock Tube Problems

We have tested the code with an MHD shock tube problem placed diagonally on a two-dimensional plane-parallel grid. The correctness and accuracy are demonstrated through the comparison of the numerical solution with the exact analytic solution from the nonlinear Riemann solver described in Ryu & Jones (1995). The calculation has been done in a box of $x = [0, 1]$ and $y = [0, 1]$, where structures propagate along the diagonal line joining $(0, 0)$ and $(1, 1)$. The initial left state is $(\rho,\ v_{\parallel},\ v_{\perp},\ v_z,\ B_{\perp},\ B_z,\ E) = (1.08,\ 1.2,\ 0.01,\ 0.5,\ 3.6/\sqrt{4\pi},\ 2/\sqrt{4\pi},\ 0.95)$ and the initial right state is $(1,\ 0,\ 0,\ 0,\ 4/\sqrt{4\pi},\ 2/\sqrt{4\pi},\ 1)$, with $B_{\parallel} = 2/\sqrt{4\pi}$. Fig. 1 shows the result. The calculation has used 256×256 cells, and plots correspond to time $t = 0.2\sqrt{2}$. The numerical solution is marked with dots, and the exact analytic solution is drawn with lines. The plotted quantities are density, gas pressure, total energy, $v_{\parallel}$ (velocity parallel to the diagonal line; i.e., parallel to the wave normal), $v_{\perp}$ (velocity perpendicular to the diagonal line but still in the computational plane), v_z (velocity in the direction out of plane), and the analogous magnetic field components, $B_{\parallel}$, $B_{\perp}$, and B_z. Fast shocks, rotational discontinuities, and slow shocks propagate from each side of the contact discontinuity, all of which

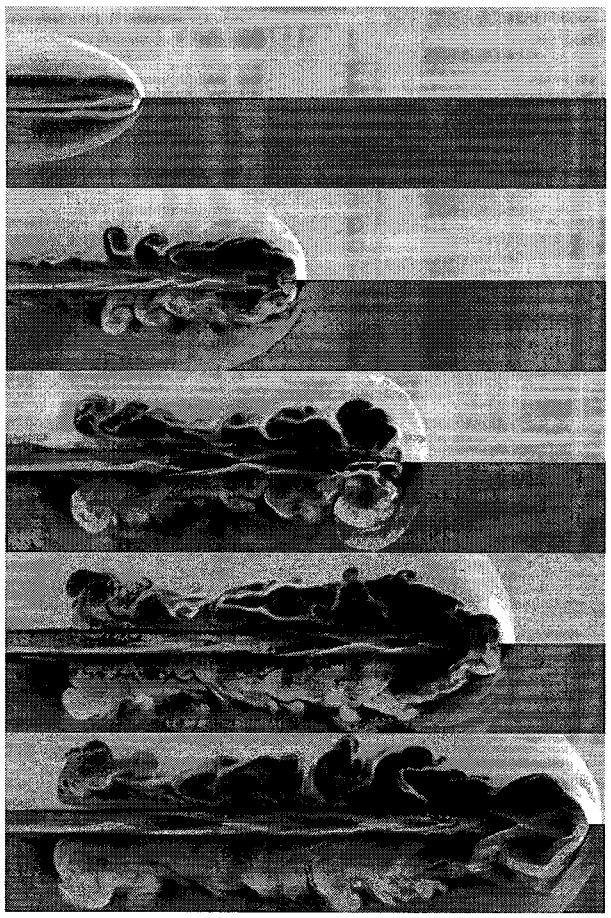

Fig. 2.— A light MHD cylindrical jet. White represents high values and black represents low values.

are correctly reproduced.

(b) Jets

We illustrate the simulation of a light cylindrical MHD jet with a top-hat velocity profile. The jet enters a cylindrical box of $r = [0, 1]$ and $z = [0, 6.64]$ at $z = 0$. The grid of the box is uniform with 256×1700 cells and the jet has a radius, r_{jet}, of 30 cells. The ambient medium has sound speed $a_{ambient} = 1$ and poloidal magnetic field ($B_\phi = B_r = 0$, $B_z = B_{ambient}$) with magnetic pressure 1% of gas pressure (plasma $\beta_{ambient} = 100$). The jet has Mach number $M_{jet} \equiv v_{jet}/a_{ambient} = 20$, gas density contrast $\rho_{jet}/\rho_{ambient} = 0.1$, and gas pressure in equilibrium with that of the ambient medium. It carries a helical magnetic field with $B_r = 0$, $B_\phi = 2 \times B_{ambient}(r/r_{jet})$, and $B_z = B_{ambient}$.

Fig. 2 shows the images of the log of the gas density and total magnetic field pressure at five different epochs, $t = 0.3$, 0.8, 1.3 1.8, and 2.2. The figure exhibits the complexity and unsteadiness of the flows. The most noticeable structures are the bow shock of the ambient medium and the terminal shock of the jet material. In addition, the jet material expands and then refocuses alternately as it flows and creates several internal oblique shock. The terminal and oblique shocks are neither steady nor stationary structures. The oblique shocks interact episodically with the terminal shock, resulting in disruption and reformation of the terminal shocks. The terminal shock includes a Mach stem, so that the jet material near the outside of the jet exits through the oblique portion of the shock. That material carries vorticity and forms a cocoon around the jet. The vorticity is further developed into complicated turbulent flows in the jet boundary layer, which is subject to the Kelvin-Helmholtz instability. There are distinct episodes of strong vortex shedding which coincide with disruption and reformation of the terminal shock. Its remnants are visible as rolls in the figure.

ACKNOWLEDGEMENTS

This work was supported in part by KRF through grant KRF-2000-015-DS0046.

REFERENCES

Balsara, D. S. 1998, ApJS, 116, 119

Balsara, D. S. & Spicer, D. S. 1999, J. Comput. Phys., 149, 270

Brio, M., & Wu, C. C. 1988, J. Comput. Phys., 75, 400

Dai, W., & Woodward P. R. 1994a, J. Comput. Phys., 111, 354

Dai, W., & Woodward P. R. 1994b, J. Comput. Phys., 115, 485

Dai, W., & Woodward P. R. 1998, ApJ, 494, 317

Harten, A. 1983, J. Comput. Phys., 49, 357

Jiang, G.-S., & Wu, C.-C. 1999, J. Comput. Phys., 150, 561

Kim, J., Ryu, D., Jones, T. W., & Hong, S. 1999, ApJ, 514, 506

Londrillo, P., & Del Zanna, L. 2000, ApJ, 530, 508

Powell, K. G. 1994, ICASE Report No. 94-24, NASA Langley Research Center

Powell, K. G., Roe, P. L., Myong, R. S., Combosi, T., & De Zeeuw, D. 1995, in Numerical Methods for Fluid Dynamics, ed. K. W. Morton & M. J. Baines (Oxford: Clarendon), 163

Roe, P. L. 1981, J. Comput. Phys., 43, 357

Roe, P. L., & Balsara, D. S. 1996, SIAM, J. Appl. Math., 56, 57

Ryu, D., & Jones, T. W. 1995, ApJ, 442, 228

Ryu, D., Jones, T. W., & Frank, A. 1995, ApJ, 452, 785

Ryu, D., Miniati, F., Jones, T. W., & Frank, A. 1998, ApJ, 509, 244

Tóth, G. 1997, Lecture Notes in Computer Science, Springer-Verlag, V. 1225, p. 253

Zachary A. L., & Colella P. 1992, J. of Comput. Phys., 99, 341

Zachary A. L., Malagoli, A., & Colella P. 1994, Siam. J. Sci. Comput., 15, 263